Chemical Science

ROYAL SOCIETY OF CHEMISTRY

EDGE ARTICLE

View Article Online
View Journal | View Issue

Cite this: *Chem. Sci.*, 2023, **14**, 9095

All publication charges for this article have been paid for by the Royal Society of Chemistry

Received 27th March 2023
Accepted 2nd August 2023

DOI: 10.1039/d3sc01597a

rsc.li/chemical-science

A GPX4-targeted photosensitizer to reverse hypoxia-induced inhibition of ferroptosis for non-small cell lung cancer therapy†

Qiao Hu,[a] Wanjie Zhu,[a] Jianjun Du, *[ab] Haoying Ge,[a] Jiazhu Zheng,[a] Saran Long,[ab] Jiangli Fan [ab] and Xiaojun Peng [a]

Ferroptosis therapy is gradually becoming a new strategy for the treatment of non-small cell lung cancer (NSCLC) because of its active iron metabolism. Because the hypoxic microenvironment in NSCLC inhibits ferroptosis heavily, the therapeutic effect of some ferroptosis inducers is severely limited. To address this issue, this work describes a promising photosensitizer **ENBS-ML210** and its application against hypoxia of NSCLC treatment based on type I photodynamic therapy and glutathione peroxidase 4 (GPX4)-targeted ferroptosis. **ENBS-ML210** can promote lipid peroxidation and reduce GPX4 expression by generating superoxide anion radicals under 660 nm light irradiation, which reverses the hypoxia-induced resistance of ferroptosis and effectively kills H1299 tumor cells. Finally, the excellent synergistic antitumor effects are confirmed both *in vitro* and *in vivo*. We firmly believe that this method will provide a new direction for the clinical treatment of NSCLC in the future.

Introduction

Non-small cell lung cancer (NSCLC) accounts for more than 80% of lung cancers,[1] and the majority of NSLCC patients are found to be in advanced inoperable stages.[2] Up to now, the clinical treatment of NSCLC has mainly depended on chemotherapeutic agents,[3] which suffers from drug resistance and side effects.[4,5] Recently, high levels of iron metabolism have been found in NSCLC, which is positive for inducing iron-dependent lipid peroxidation and finally ferroptosis, which is becoming a new strategy for NSCLC therapy.[6,7] Glutathione peroxidase 4 (GPX4), which is overexpressed in NSCLC and specifically converts lipid peroxides (LPO) into lipoid alcohols, plays important roles in the regulation of ferroptosis.[8–11] Though GPX4 inhibitors have been used to trigger ferroptosis,[12,13] the hypoxia microenvironment, existing in most solid tumors, restricts ferroptosis heavily because hypoxia inducible factors inhibit ferritinophagy and thus reduce the free iron pool and reactive oxygen species, preventing cells from undergoing ferroptosis.[14–16] Therefore, addressing the hypoxia-induced inhibition to ferroptosis in NSCLC therapy deserves much attention.

Photodynamic therapy (PDT) is a charming method in tumor treatment because of its minimal invasiveness, non-drug resistance, controllable therapeutic area and so forth. In principle, reactive oxygen species (ROS), produced in PDT, can promote intracellular lipid peroxidation.[17,18] However, among the ROS, $^1O_2$, produced by typical type II photosensitizers (*e.g.* Ce6 and porphyrin),[19–31] contributes little to LPO formation. Conversely, the radicals (*e.g.* superoxide anion radicals ($\cdot O_2^-$) and hydroxyl radicals ($\cdot OH$))[32–34] formed in type I PDT did well in oxidizing lipids even under hypoxic conditions.[35–37] However, successful examples of type I PDT-synergistic ferroptosis have been rare in NSCLC therapy.

In our former work, a GPX4-targeting probe **ENBO-ML210** was reported for the selective imaging of NSCLC, wherein the introduction of fluorophore **ENBO** did not affect the interaction of inhibitor ML210 with GPX4.[38] Additionally, previous research about the type I photosensitizer **ENBS** is generally considered to indicate hypoxia tolerance.[33] Inspired by **ENBO-ML210**, herein, **ENBS-ML210** was developed, using type I photosensitizer **ENBS** instead of **ENBO**, as a GPX4-targeting photosensitizer for NSCLC therapy (Scheme 1). Under 660 nm light irradiation, **ENBS-ML210** produced $\cdot O_2^-$ to induce lipid peroxidation and reduce GPX4 expression with more than 70% cell death rate under both normoxic and hypoxic conditions. This ingenious strategy provides a paradigm for the development of ferroptosis-based NSCLC therapy with hypoxia.

[a]*State Key Laboratory of Fine Chemicals, Frontiers Science Center for Smart Materials Oriented Chemical Engineering, School of Chemical Engineering, Dalian University of Technology, Dalian 116024, China. E-mail: dujj@dlut.edu.cn*

[b]*Ningbo Institute of Dalian University of Technology, 26 Yucai Road, Jiangbei District, Ningbo 315016, P. R. China*

† Electronic supplementary information (ESI) available: Experimental methods, syntheses and structure characterization, and figures. See DOI: https://doi.org/10.1039/d3sc01597a

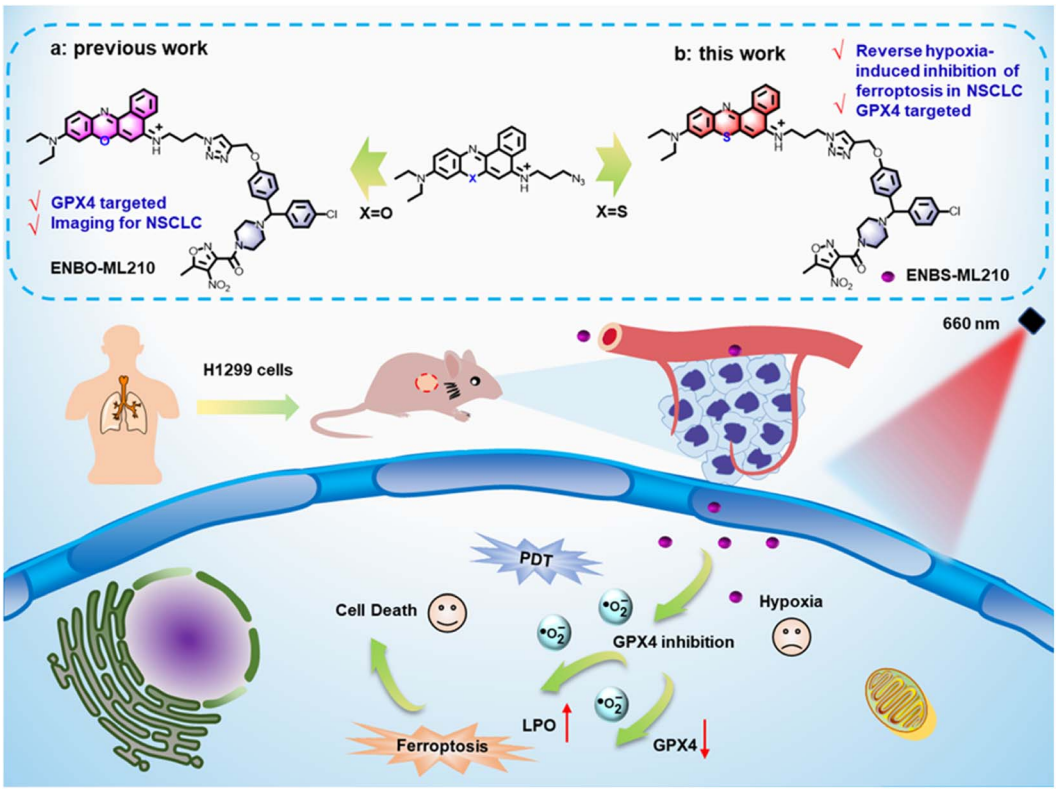

Scheme 1 Schematic illustration of the molecular design of **ENBS-ML210** and mechanism of reversing hypoxia-induced inhibition of ferroptosis in H1299 cells.

Results and discussion

Synthesis and characterization of ENBS-ML210

ENBS-ML210 was synthesized and confirmed by ^{1}H and ^{13}C nuclear magnetic resonance (NMR) and high-resolution mass spectrometry (HRMS) (Fig. S1–S7†). As shown in Fig. 1A, **ENBS-ML210** exhibited similar UV-vis absorption and fluorescence emission (600–700 nm) to **ENBS**. Density functional theory (DFT) calculations were performed at the B3LYP/6-31g(d) level with Gaussian 09 (Fig. S8†), and the ΔE_g between the HOMO and LUMO of **ENBS-ML210** (2.38 eV) is similar to that of **ENBS** (ΔE_g = 2.39 eV). In addition, the UV-vis absorption and fluorescence spectra of **ENBS-ML210** were still in the NIR window in different solvents (Fig. S9 and S10†). The generation of ROS by **ENBS-ML210** was evaluated by using 1,3-diphenylisobenzofuran (DPBF). As shown in Fig. 1B, the absorbance of DPBF at 415 nm decreased dramatically under both 21% and 2% oxygen conditions under 660 nm light irradiation (Fig. S11†), indicating little O_2 dependence. Furthermore, a dihydrorhodamine 123 (DHR123) fluorescence probe was used as a specific $\cdot O_2^-$ probe. The green fluorescence intensity at 526 nm (DHR123) distinctly increased under 660 nm light irradiation (Fig. 1C), indicating that **ENBS-ML210** has a good ability to produce $\cdot O_2^-$ as a type I photosensitizer. To further detect and differentiate between $\cdot O_2^-$, $^{1}O_2$ and $\cdot$OH, electron paramagnetic resonance (EPR) spectroscopy was performed in which $\cdot O_2^-$ and $\cdot$OH were trapped by 5,5-dimethyl-1-propylamine-*n*-oxide (DMPO) ($\cdot O_2^-$ was in MeOH and $\cdot$OH was in H_2O), and $^{1}O_2$ was trapped by 2,2,6,6-tetramethylpiperidine (TEMP). As shown in Fig. 1D, compared with those of the control and **ENBS-ML210** groups, the **ENBS-ML210** + light group displayed strong $\cdot O_2^-$ and weak $\cdot$OH signals, and hardly generated $^{1}O_2$.

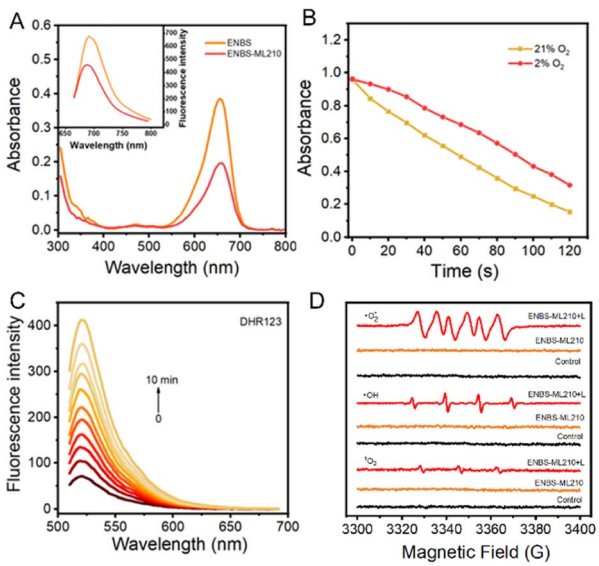

Fig. 1 Spectral properties and ROS generation of **ENBS-ML210**. (A) UV-vis absorption and fluorescence spectra of **ENBS** and **ENBS-ML210**. (B) The absorbance at 415 nm of DPBF degradation with **ENBS-ML210** under 21% O_2 and 2% O_2 conditions. (C) Fluorescence spectra of DHR123 for $\cdot O_2^-$ detection. (D)EPR spectra of $\cdot O_2^-$, $\cdot$OH, and $^{1}O_2$ in the control, **ENBS-ML210**, and **ENBS-ML210** + light groups.

Cell uptake and ROS generation

The uptake level of small molecule drugs and their localization in tumor cells are the key factors to determine the antitumor effect. As shown in Fig. 2A, real-time uptake imaging of **ENBS-ML210** was performed in H1299 cells. With the prolongation of incubation time, the red fluorescence intensity gradually increased and reached the maximum after 90 min. Furthermore, a long retention time of **ENBS-ML210** of at least 360 min was observed in H1299 cells (Fig. 2B). Subsequently, subcellular localization imaging showed that the fluorescence of **ENBS-ML210** was well overlapped with that of the lysosomal staining agent LysoTracker (Pearson's coefficient: 0.922), which is much better than MitoTracker in mitochondria (0.695) and Hoechst 33342 in the nucleus (0.098) (Fig. 2C). Moreover, an immunocyto-fluorescence assay was introduced to analyze the cellular colocalization of **ENBS-ML210** with GPX4 using an Alexaflour 488-labeled fluorescent secondary antibody. As shown in Fig. S12,† GPX4 staining with its fluorescent secondary antibody showed green fluorescence, which was well colocalized with the red fluorescence of **ENBS-ML210** (Pearson's coefficients: 0.832). The above results demonstrated that **ENBS-ML210** mainly targeted GPX4 in lysosomal membranes of H1299 cells.

The ROS generation of **ENBS-ML210** was explored *in vitro*. As shown in Fig. 2D, using 2,7-dichlorodihydrofluorescein diacetate (DCFH-DA) as a universal indicator of ROS, the intracellular signal intensity of green fluorescence increased obviously under light irradiation (660 nm and 20 mW cm^{-2}), suggesting efficient ROS generation of **ENBS-ML210**. Furthermore, dihydroethidium (DHE), singlet oxygen sensor green reagent (SOSG), and hydroxyphenyl fluorescein (HPF) were used to detect intracellular $\cdot O_2^-$, $^1O_2$ and $\cdot OH$, respectively. The results showed that **ENBS-ML210** exhibited an excellent capability in generating $\cdot O_2^-$ *in vitro*, and it also produced a small amount of $\cdot OH$.

Study about the effect of hypoxia on ferroptosis

Determining the effect of hypoxia on ferroptosis is crucial for the treatment of NSCLC. ML210 was introduced as a ferroptosis inducer in MCF-7 (human breast cancer cells), 4T1 (mouse breast cancer cells), and H1299 cells (human non-small cell lung cancer cells) under normoxia (21% O_2) and hypoxia (2% O_2), respectively. As shown in Fig. 3A and B, when ML210 was 10 μM, the cell survival rates of MCF-7 cells were 73% (normoxia) and 83% (hypoxia), and the cell survival rates of 4T1 cells changed little whether under normoxia or hypoxia conditions. Interestingly, we found the cell survival rate of H1299 cells exhibited obvious change between normoxia conditions (40%) and hypoxia conditions (79%), suggesting that hypoxia could significantly inhibit ferroptosis (Fig. 3C and S13†). Next, we evaluated the expression of GPX4 protein in MCF-7, 4T1, and H1299 cells by western blotting. As shown in Fig. 3D, GPX4 protein was expressed in three kinds of cells, and was most

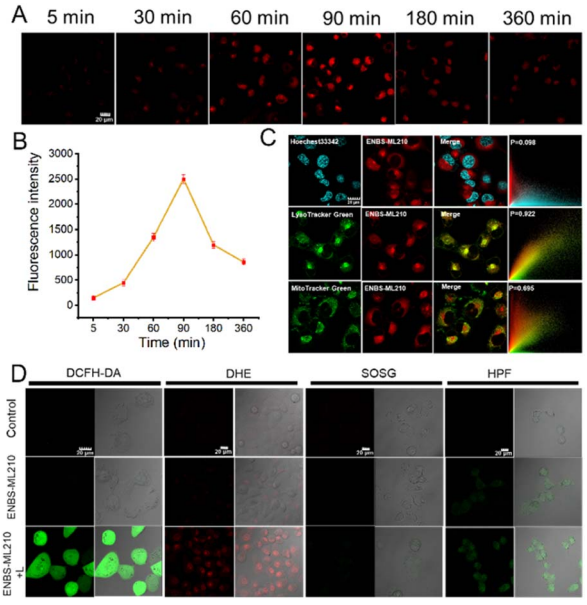

Fig. 2 *In vitro* cell imaging of **ENBS-ML210**. (A) Cell uptake imaging and (B) quantitative analysis of **ENBS-ML210** in H1299 cells. (C) Subcellular localization imaging of **ENBS-ML210** in H1299 cells (**ENBS-ML210**: λ_{ex} = 640 nm and λ_{em} = 650–750 nm; Hoechst 33342: λ_{ex} = 405 nm and λ_{em} = 440–480 nm; MitoTracker Green: λ_{ex} = 488 nm and λ_{em} = 500–550 nm; LysoTracker Green: λ_{ex} = 488 nm and λ_{em} = 500–550 nm; scale bar = 20 μm). (D) Intracellular ROS detection of total intracellular ROS, $\cdot O_2^-$, $^1O_2$, and $\cdot OH$, using DCFH-DA, DHE, SOSG and HPF as fluorescence indicators.

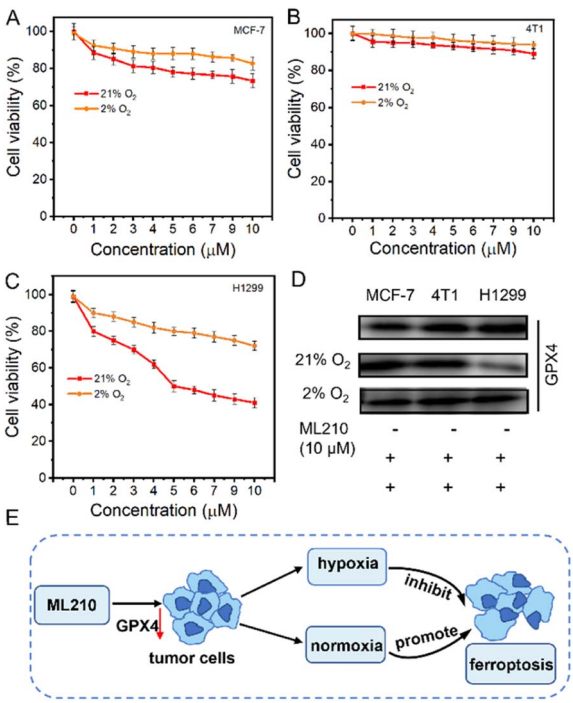

Fig. 3 The relationship between ferroptosis and oxygen conditions. The cytotoxicity of the GPX4 inhibitor ML210yne in (A) MCF-7, (B) 4T1, and (C) H1299 cells under 21% and 2% O_2 conditions. (D) Western blot analysis of the expression of GPX4 with 10 μM ML210 in MCF-7, 4T1, and H1299 cells under 21% O_2 and 2% O_2 conditions. (E) Schematic diagram of the effect of ML210 on ferroptosis for tumor cells under normoxia and hypoxia. $^{**}P < 0.01$ determined by Student's-test.

expressed in H1299 cells. The three kinds of cells were treated with 10 μM ML210 under normoxic (21% O_2) and hypoxic (2% O_2) conditions, respectively. The expression of GPX4 in H1299 cells was significantly reduced under normoxia, while the expression of GPX4 was hardly reduced under hypoxia. The above results showed that ferroptosis was inhibited under hypoxia. The process of the effect of hypoxia on ferroptosis in tumor cells is shown in Fig. 3E. ML210, a ferroptosis inducer, inhibited the overexpression of GPX4 in tumor cells, and ferroptosis was inhibited under hypoxia because the reduction of ROS was not conducive to ferritinophagy.[14] In contrast, ferroptosis could occur normally under normoxia. Therefore, to overcome this shortcoming of ML210, **ENBS-ML210** was developed to reverse hypoxia-induced inhibition of ferroptosis in NSCLC.

Mechanism of reversing ferroptosis resistance *in vitro*

The inactivation of GPX4 could lead to the accumulation of lipid peroxides, which is an important sign of ferroptosis. To explore the generation of LPO, the fluorescence of C11-BODIPY was introduced as a LPO probe by CLSM. As shown in Fig. 4A, under 21% O_2 conditions, stronger green fluorescence was observed in the ML210 and **ENBS-ML210** groups, while very weak green fluorescence was observed in the control groups. In addition, the green fluorescence almost disappeared in the ML210 group under 2% O_2 conditions, while green fluorescence was displayed by the **ENBS-ML210** + light group, indicating that **ENBS-ML210** could reverse hypoxia-induced inhibition of ferroptosis. **ENBS-ML210** could lead to lipid peroxidation by reducing the expression of GPX4 and the generation of ROS under light irradiation. Furthermore, as shown in Fig. 4B and C, the **ENBS-ML210** + light group displayed 15-fold and 7.7-fold stronger fluorescence intensity than the control group under 21% O_2 and 2% O_2 conditions, respectively, while the **ENBS** + light group showed 5-fold stronger fluorescence intensity compared with the control group, showing that **ENBS-ML210** could promote ferroptosis through PDT-induced ROS. The cell death was verified using a cell live/dead stain test. As expected, **ENBS-ML210** induced complete destruction of H1299 cells after 660 nm light irradiation compared with control and **ENBS** groups (Fig. S14†). Moreover, FITC-Annexin V/PI double-staining revealed that both **ENBS** and **ENBS-ML210** were able to induce apoptosis and necrosis upon irradiation (Fig. S15†).

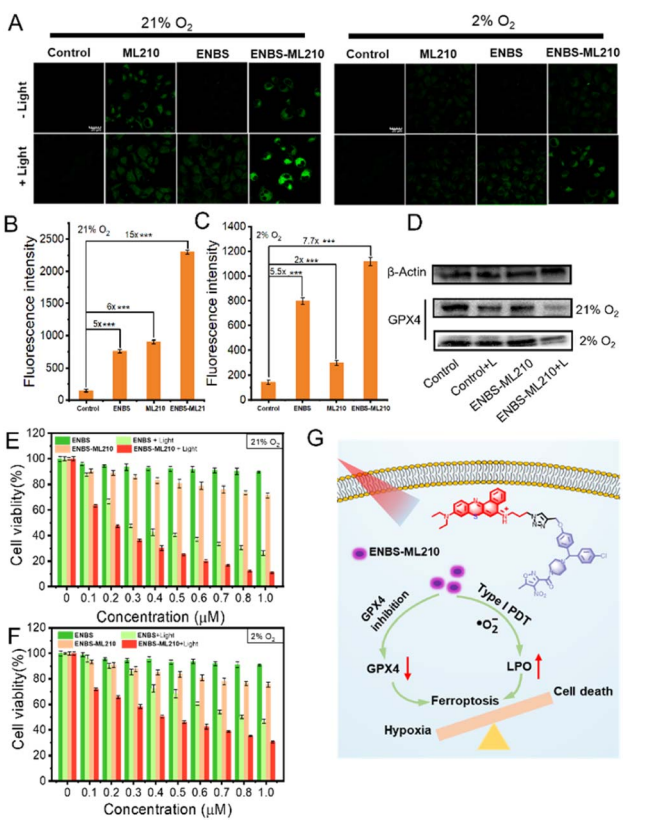

Fig. 4 The mechanism of PDT-promoted ferroptosis in H1299 cells. (A) Lipid peroxidation measurement of H1299 cells under different treatments by CLSM. Representation of the fluorescence intensity of C11 BODIPY obtained from the microscopy images under (B) 21% O_2 and (C) 2% conditions. (D) Western blot analysis of the expression of GPX4 in different treatment groups. MTT assay to assess the cell viability of H1299 cells with different treatments under (E) 21% O_2 and (F) 2% O_2 conditions. (G) Summarized mechanisms of reversing ferroptosis resistance by type I PDT. ***P < 0.001 determined by Student's-test.

Western blotting with **ENBS-ML210** revealed that the intracellular GPX4 protein expression was reduced under light irradiation under 21% O_2 and 2% O_2 conditions (Fig. 4D). In addition, the expression of GPX4 protein with the **ENBS-ML210** + light group was less under normoxia than that under hypoxia, indicating that hypoxia may inhibit ferroptosis. The cytotoxicity of **ENBS-ML210** at different oxygen levels was investigated using 3-(4,5-dimethylthiazol-2-yl)-2,5-diphenyltetrazolium bromide (MTT) assay to explore the therapeutic effect. As shown in Fig. S16,† **ENBS-ML210** exhibited weak cytotoxicity to COS-7 cells, while the killing effects on MCF and 4T1 cells were obvious (IC_{50} = 0.51 μM and IC_{50} = 0.62 μM, respectively). Importantly, as shown in Fig. 4E, under normoxic conditions (21% O_2), the IC_{50} value of **ENBS-ML210** reached 0.19 μM under light irradiation, which was better than that of **ENBS** (IC_{50} = 0.28 μM). Furthermore, the cell survival rate was as low as 30% for **ENBS-ML210** (1 μM) under hypoxic conditions (2% O_2), indicating its good therapeutic effect under hypoxia (Fig. 4F). The above results showed that **ENBS-ML210** has good killing selectivity toward H1299 cells. In general, a simple schematic diagram of the synergistic mechanism of reversing ferroptosis resistance by type I PDT is shown in Fig. 4G. Obviously, ferroptosis is inhibited under hypoxia conditions. **ENBS-ML210** could lead to the reduction of GPX4, and promoted lipid peroxidation through the generation of $\cdot O_2^-$ by type I PDT under light irradiation, thus promoting the ferroptosis of tumor cells.

Antitumor study *in vivo*

The excellent tumoricidal efficiency of **ENBS-ML210** at the cell level encouraged us to further evaluate the therapeutic effect *in vivo*. H1299 xenograft Balb/c nude mice were used as experimental models. Before evaluating the antitumor effect of **ENBS-**

ML210, the enrichment capacity in tumors was tested. As shown in Fig. S17A and B,† the enrichment of **ENBS-ML210** in tumors was better than that in any other organs (Fig. S17C and D†), indicating that **ENBS-ML210** efficiently targeted H1299 tumors.

Capitalizing on this, further antitumor experiments were performed (Fig. 5A). H1299 tumor-bearing nude mice were randomly divided into five groups ($n = 5$) and had their tail vein injected with different reagents: (1) control, (2) **ENBS**, (3) **ENBS** + light (660 nm, 100 mW cm^{-2}, and 15 min), (4) **ENBS-ML210**, and (5) **ENBS-ML210** + light. The tumor volume and weight of mice were recorded every other day. After 14 days of treatment, the *in vivo* antitumor effects of different treatments are shown in Fig. 5B and S18.† An obvious tumor growth was observed in the group (1) and group (2) (≈10-fold), while the group (5) showed a more remarkable tumor-inhibition rate of 95.2% than that in group (3) (72.6%). The body weight of mice did not change abnormally during treatment (Fig. 5C and S19†). The average tumor weight and representative tumor images also confirmed the excellent antitumor performance (Fig. 5D–F). As shown in the H&E staining (Fig. 5G), large quantities of tumor cells lost their cellular integrity only in group (5). Moreover, group (5) also exhibited the strongest immunofluorescence green signal in TUNEL staining, which illustrated the maximum cell apoptosis. The histological examination of all major organs by H&E staining showed no pathological alterations or other abnormalities (Fig. S20†), suggesting the biocompatibility and biosafety of **ENBS-ML210**. These results collectively demonstrated the high biocompatibility and strong antitumor effect of **ENBS-ML210** in NSCLC.

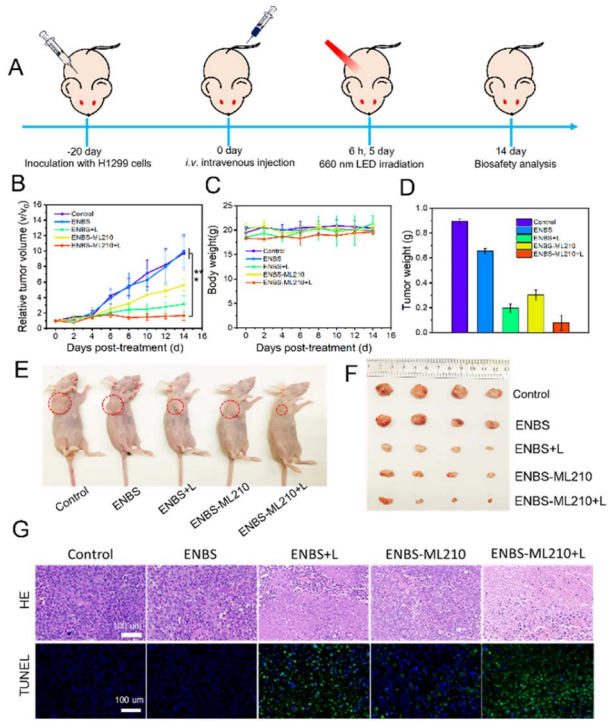

Fig. 5 *In vivo* antitumor efficacy in H1299 tumor-bearing nude mice. (A) Tumor treatment program by intravenous injection. (B) Relative tumor volume of mice after different treatments. (C) Tumor weight of mice after different treatments. (D) Average weight of tumors for mice at 14 days post-treatment. (E) Representative photos of mice on the 14th day of treatment. (F) Tumor photos at the end of the treatment period in different groups. (G) H&E staining and TUNEL staining of tumor slides from mice after different treatments. Scale bars = 100 μm. ***$P < 0.001$ determined by Student's-test.

Conclusions

In summary, **ENBS-ML210** was rationally designed and developed by covalently linking a photosensitizer **ENBS** with a GPX4 inhibitor ML210. **ENBS-ML210** could directly target GPX4 overexpressed in H1299 cells and generate $\cdot O_2^-$ under 660 nm light irradiation. *In vitro* results displayed that H1299 cells were killed effectively under both 21% and 2% O_2 conditions. *In vivo* experimental results showed that **ENBS-ML210** could significantly inhibit tumor growth and achieve an excellent therapeutic effect. Overall, the **ENBS-ML210** reported here demonstrates that type I PDT could reverse hypoxia-induced inhibition of ferroptosis, providing a new strategy for non-small cell lung cancer therapy.

Data availability

The ESI† includes the synthesis, NMR and high-resolution mass spectrometry of **ENBS** and **ENBS-ML210**, cell imaging, cell apoptosis analysis, detection of lipid peroxidation, western blotting, mouse phototherapy, biosafety tests, *etc.*

Author contributions

Q. Hu designed and performed all the experiments and wrote the manuscript. W. J. Zhu participated in the synthesis of some molecular intermediates. J. J. Du directed the whole process in this work, guided the writing and revised the manuscript. H. Y. Ge and J. Z. Z provided guidance on some experimental details. S. R. Long, J. L. Fan and X. J. Peng offered constructive suggestions on the improvement of this work and provided financial support.

Conflicts of interest

The authors declare no competing financial interests.

Acknowledgements

This work was financially supported by the NSFC-Liaoning United Fund (U1908202 and U21A20399), National Natural Science Foundation of China (21925802 and 22090011), Fundamental Research Funds for the Central Universities of China (DUT21ZD407, DUT21YG103 and DUT22LAB601), China Postdoctoral Science Foundation (2021M690515) and Liaoning Revitalization Talents Program (XLYC2007084). This study was conducted in accordance with the Guide for the Care and Use of Laboratory Animals published by the US National Institutes of Health (8th edition, 2011). The animal protocol was approved by the local research ethics review board of the Animal Ethics

Committee of Dalian University of Technology. The assigned approval number is 2019-016.

Notes and references

1 S. O. Dolly, D. C. Collins, R. Sundar, S. Popat and T. A. Yap, *Drugs*, 2017, **77**, 813–827.
2 Z. C. Ye, Y. M. Huang, J. H. Ke, X. Zhu, S. L. Leng and H. Luo, *Biomed. Pharmacother.*, 2021, **133**, 111079.
3 R. M. Mohammad, I. Muqbil, L. Lowe, C. Yedjou, H. Y. Hsu, L. T. Lin, M. D. Siegelin, C. Fimognari, N. B. Kumar, Q. P. Dou, H. J. Yang, A. K. Samadi, G. L. Russo, C. Spagnuolo, S. K. Ray, M. Chakrabarti, J. D. Morre, H. M. Coley, K. Honoki, H. Fujii, A. G. Georgakilas, A. Amedei, E. Niccolai, A. Amin, S. S. Ashraf, W. G. Helferich, X. J. Yang, C. S. Boosani, G. Guha, D. Bhakta, M. R. Ciriolo, K. Aquilano, S. Chen, S. I. Mohammed, W. N. Keith, A. Bilsland, D. Halicka, S. Nowsheen and A. S. Azmi, *Semin. Cancer Biol.*, 2015, **35**, S78–S103.
4 D. S. Li and Y. S. Li, *Signal Transduction Targeted Ther.*, 2020, **5**, 108.
5 T. L. Ma, Y. Zhou, C. Wang, L. Wang, J. X. Chen, H. H. Yang, C. Y. Zhang, Y. Zhou and C. X. Guan, *Oxid. Med. Cell. Longevity*, 2021, **2021**, 1098970.
6 X. J. Xia, X. P. Fan, M. Y. Zhao and P. Zhu, *Curr. Gene Ther.*, 2019, **19**, 117–124.
7 J. Y. Zou, L. Wang, H. L. Tang, X. X. Liu, F. Peng and C. Peng, *Int. J. Mol. Sci.*, 2021, **22**, 13335.
8 W. S. Yang, R. SriRamaratnam, M. E. Welsch, K. Shimada, R. Skouta, V. S. Viswanathan, J. H. Cheah, P. A. Clemons, A. F. Shamji, C. B. Clish, L. M. Brown, A. W. Girotti, V. W. Cornish, S. L. Schreiber and B. R. Stockwell, *Cell*, 2014, **156**, 317–331.
9 T. Ma, J. Du, Y. Zhang, Y. Wang, B. Wang and T. Zhang, *Cell Death Discovery*, 2022, **8**, 434.
10 D. Tang and G. Kroemer, *Curr. Biol.*, 2020, **30**, R1292–R1297.
11 X. Jiang, B. R. Stockwell and M. Conrad, *Nat. Rev. Mol. Cell Biol.*, 2021, **22**, 266–282.
12 J. K. Eaton, R. A. Ruberto, A. Kramm, V. S. Viswanathan and S. L. Schreiber, *J. Am. Chem. Soc.*, 2019, **141**, 20407–20415.
13 X. Y. Zhao, J. Y. Zhang, W. Zhang, Z. J. Guo, W. Wei, X. X. Wang and J. Zhao, *Chem. Sci.*, 2023, **14**, 1114–1122.
14 S. Ni, Y. Yuan, Z. Qian, Z. Y. Zhong, T. Lv, Y. B. Kuang and B. Q. Yu, *Free Radical Biol. Med.*, 2021, **169**, 271–282.
15 Y. T. Bai, F. J. Xiao, H. Wang, R. L. Ge and L. S. Wang, *Int. J. Med. Sci.*, 2021, **18**, 1618–1627.
16 Z. Dong, P. Liang, G. Guan, B. Yin, Y. Wang, R. Yue, X. Zhang and G. Song, *Angew. Chem., Int. Ed.*, 2022, **61**, e202206074.
17 L. Ke, F. Wei, L. Xie, J. Karges, Y. Chen, L. Ji and H. Chao, *Angew. Chem., Int. Ed.*, 2022, **61**, e202205429.
18 X. Li, S. Lee and J. Yoon, *Chem. Soc. Rev.*, 2018, **47**, 1174–1188.
19 J. W. Huang, S. Wang, Y. Zhou, Q. X. Li, J. Yin, D. L. Zha, J. Y. Zhong, W. M. Zhou, C. K. Zheng, Y. L. Miao, W. J. Chen, C. S. Xu, Y. L. Li and T. Gong, *Chem. Eng. J.*, 2023, **451**, 138585.
20 X. L. Liang, M. Chen, P. Bhattarai, S. Hameed, Y. D. Tang and Z. F. Dal, *ACS Nano*, 2021, **15**, 20164–20180.
21 L. P. Zhao, S. Y. Chen, R. R. Zheng, X. N. Rao, R. J. Kong, C. Y. Huang, Y. B. Liu, Y. Z. Tang, H. Cheng and S. Y. Li, *ACS Appl. Mater. Interfaces*, 2022, **14**, 53501–53510.
22 J. Chen, F. Chen, L. Zhang, Z. Y. Yang, T. Deng, Y. F. Zhao, T. Y. Zheng, X. L. Gan, H. T. Zhong, Y. Q. Geng, X. W. Fu, Y. Q. Wang and C. Yu, *ACS Appl. Mater. Interfaces*, 2021, **13**, 27856–27867.
23 R. Sun, W. Ma, M. J. Ling, C. H. Tang, M. Zhong, J. Y. Dai, M. Y. Zhu, X. Z. Cai, G. Li, Q. Xu, L. G. Tang, Z. Q. Yu and Z. W. Peng, *J. Controlled Release*, 2022, **350**, 525–537.
24 X. Yu, Y.-C. Zhang, X. Yang, Z. Huang, T. Zhang, L. Yang, W. Meng, X. Liu, P. Gong, A. Forni, Z. Zheng, B. Liu, P. Zhang, L. Cai and B. Z. Tang, *Nano Today*, 2022, **44**, 101477.
25 F. Wei, J. Karges, J. Shen, L. Xie, K. Xiong, X. Zhang, L. Ji and H. Chao, *Nano Today*, 2022, **44**, 101509.
26 W. L. Pan, Y. Tan, W. Meng, N. H. Huang, Y. B. Zhao, Z. Q. Yu, Z. Huang, W. H. Zhang, B. Sun and J. X. Chen, *Biomaterials*, 2022, **283**, 121449.
27 S. Saita and H. Kawasaki, *Luminescence*, 2023, **38**, 127–135.
28 L. W. Zhu, Y. C. You, M. X. Zhu, Y. L. Song, J. C. Zhang, J. H. Hu, X. Y. Xu, X. L. Xu, Y. Z. Du and J. S. Ji, *Adv. Mater.*, 2022, **34**, 2207174.
29 F. T. Yang, W. J. Yu, Q. Y. Yu, X. Y. Liu, C. P. Liu, C. Lu, X. H. Liao, Y. Liu and N. Peng, *Small*, 2023, **19**, 2206124.
30 L. L. Shi, P. Zhang, X. X. Liu, Y. Z. Li, W. B. Wu, X. H. Gao and B. Liu, *Adv. Mater.*, 2022, **34**, 2207174.
31 R. D. Song, T. L. Li, J. Y. Ye, F. Sun, B. Hou, M. Saeed, J. Gao, Y. J. Wang, Q. W. Zhu, Z. Xu and H. J. Yu, *Adv. Mater.*, 2021, **33**, 2101155.
32 X. Li, N. Kwon, T. Guo, Z. Liu and J. Yoon, *Angew. Chem., Int. Ed.*, 2018, **57**, 11522–11531.
33 M. L. Li, J. Xia, R. S. Tian, J. Y. Wang, J. L. Fan, J. J. Du, S. Long, X. Z. Song, J. W. Foley and X. J. Peng, *J. Am. Chem. Soc.*, 2018, **140**, 14851–14859.
34 M. L. Li, T. Xiong, J. J. Du, R. S. Tian, M. Xiao, L. Y. Guo, S. R. Long, J. L. Fan, W. Sun, K. Shao, X. Z. Song, J. W. Foley and X. J. Peng, *J. Am. Chem. Soc.*, 2019, **141**, 2695–2702.
35 D. P. Chen, Q. Xu, W. J. Wang, J. J. Shao, W. Huang and X. C. Dong, *Small*, 2021, **17**, 2006742.
36 Y. Y. Wang, Y. C. Liu, H. W. Sun and D. S. Guo, *Coord. Chem. Rev.*, 2019, **395**, 46–62.
37 L. Yu, Y. Xu, Z. J. Pu, H. Kang, M. Li, J. L. Sessler and J. S. Kim, *J. Am. Chem. Soc.*, 2022, **144**, 11326–11337.
38 Q. Hu, W. J. Zhu, J. J. Du, S. R. Long, W. Sun, J. L. Fan and X. J. Peng, *Chem. Commun.*, 2023, **59**, 294–297.